Temperature and Water Vapor Variance Scaling in Global Models: Comparisons to Satellite and Aircraft Data

B. H. KAHN,* J. TEIXEIRA,* E. J. FETZER,* A. GETTELMAN,+ S. M. HRISTOVA-VELEVA,* X. HUANG,# A. K. KOCHANSKI,@ M. KÖHLER,& S. K. KRUEGER,@ R. WOOD,** AND M. ZHAO++

* *Jet Propulsion Laboratory, California Institute of Technology, Pasadena, California*
+ *National Center for Atmospheric Research, Boulder, Colorado*
# *Department of Atmospheric, Oceanic and Space Sciences, University of Michigan, Ann Arbor, Michigan*
@ *Department of Atmospheric Sciences, University of Utah, Salt Lake City, Utah*
& *Deutscher Wetterdienst, Offenbach, Germany*
** *Department of Atmospheric Sciences, University of Washington, Seattle, Washington*
++ *Geophysical Fluid Dynamics Laboratory, Princeton, New Jersey*

(Manuscript received 30 December 2010, in final form 3 March 2011)

ABSTRACT

Observations of the scale dependence of height-resolved temperature T and water vapor q variability are valuable for improved subgrid-scale climate model parameterizations and model evaluation. Variance spectral benchmarks for T and q obtained from the Atmospheric Infrared Sounder (AIRS) are compared to those generated by state-of-the-art numerical weather prediction ''analyses'' and ''free-running'' climate model simulations with spatial resolution comparable to AIRS. The T and q spectra from both types of models are generally too steep, with small-scale variance up to several factors smaller than AIRS. However, the two model analyses more closely resemble AIRS than the two free-running model simulations. Scaling exponents obtained for AIRS column water vapor (CWV) and height-resolved layers of q are also compared to the superparameterized Community Atmospheric Model (SP-CAM), highlighting large differences in the magnitude of CWV variance and the relative flatness of height-resolved q scaling in SP-CAM. Height-resolved q spectra obtained from aircraft observations during the Variability of the American Monsoon Systems Ocean–Cloud–Atmosphere–Land Study Regional Experiment (VOCALS-REx) demonstrate changes in scaling exponents that depend on the observations' proximity to the base of the subsidence inversion with scale breaks that occur at approximately the dominant cloud scale (~10–30 km). This suggests that finer spatial resolution requirements must be considered for future satellite observations of T and q than those currently planned for infrared and microwave satellite sounders.

1. Introduction

The scale dependences of atmospheric horizontal winds, potential temperature θ, and kinetic energy (KE) power spectra obtained from aircraft observations follow an approximate -3 power-law wavenumber scaling for length scales less than 800 km (and $-5/3$ for scales greater than 500 km) (e.g., Nastrom and Gage 1985), but a complete physical explanation of their origin continues to be vigorously debated (e.g., Tung and Orlando 2003; Tulloch and Smith 2006; Lindborg 2009; Lindborg et al. 2010; Lovejoy et al. 2009; Smith and Tulloch 2009; Tuck 2010). Observational benchmarks of scaling exponents have been used to evaluate KE spectra obtained from relatively low- (Koshyk et al. 1999) and high-resolution (Skamarock 2004; Takahashi et al. 2006; Hamilton et al. 2008) NWP and climate models in order to gain insights into model physics and determine whether the -3 to $-5/3$ break in the mesoscale region is faithfully represented.

Most of the emphasis in the literature to date focuses on comparisons of KE spectra between observations and models (Hamilton et al. 2008). The scale dependences of the variability of temperature T and especially water vapor q are not well characterized in space and time on a global basis despite both variables strongly controlling cloud processes at the subgrid scale in NWP and climate models (Cusack et al. 1999; Tompkins 2002; Seiffert and

Corresponding author address: Brian H. Kahn, Jet Propulsion Laboratory, 4800 Oak Grove Drive, Mail Stop 169-237, Pasadena, CA 91109.
E-mail: brian.h.kahn@jpl.nasa.gov

DOI: 10.1175/2011JAS3737.1

von Storch 2008; Wang et al. 2010) and therefore helping to establish the sign and magnitude of cloud feedbacks and overall climate sensitivity (Randall et al. 2007). Furthermore, the few existing aircraft studies of q spectra in the mesoscale (e.g., Nastrom et al. 1986; Cho et al. 2000) support an approximate -2 scaling with little or no mesoscale break reported, in stark contrast to previously published potential temperature and KE spectra.

Recently, Kahn and Teixeira (2009, hereafter KT09) derived a global observationally based climatology of T and q variance scaling from the Atmospheric Infrared Sounder (AIRS) Advanced Microwave Sounding Unit (AMSU) (hereafter simply AIRS) suite between ~150 and 1300 km. A rich variety of structure in the scaling exponents was revealed from these observations that were not previously reported from aircraft (e.g., Nastrom and Gage 1985) and satellite observational studies (e.g., Cahalan et al. 1994) owing to aircraft sampling limitations and ambiguities in interpreting raw satellite radiances (KT09). Geophysical products obtained from satellite sounders and imagers are potentially very powerful because of their ability to represent a scale-dependent probability distribution function (PDF) over orders of magnitude in spatial scale, depending on the sensor spatial resolution and swath characteristics, with near-global sampling coverage. Furthermore, the scale dependence of joint PDFs of T and q control the distributions of cloud condensate (e.g., Kawai and Teixeira 2010; Wang et al. 2010) and magnitude of climate sensitivity (e.g., Kuwano-Yoshida et al. 2010). Wood et al. (2002) showed with aircraft data the cloud fraction (CF) in a nominal climate model grid box is reasonably approximated by the mean saturation excess divided by its variance. (The mean saturation excess is the difference between a grid box–averaged total water content and saturation specific humidity.) As a result, an excess (or lack of) T and/or q variance will limit a model's ability to generate a realistic CF. For example, an excess of (or lack of) variance produces a broader (narrower) probability distribution function of CF at a similar spatial scale of T and q variance (Wood and Field 2011).

In this paper, scaling exponents derived from AIRS, two contemporary NWP model analyses, two "free-running" climate models, one "superparameterized" climate model, and aircraft data from the Variability of the American Monsoon Systems Ocean–Cloud–Atmosphere–Land Study Regional Experiment (VOCALS-REx) (Wood et al. 2011) are described, where AIRS and model horizontal resolutions are comparable. Although many published studies of aircraft-based turbulence spectra exist, especially with regard to the free troposphere (e.g., Nastrom and Gage 1985), the present paper emphasizes VOCALS-REx data within stratocumulus because of its large potential contribution to cloud–climate feedback (Bony and Dufresne 2005). In this diagnostic study, we will show that the climate and NWP models evaluated herein tend to underestimate small-scale variance of T and q, but important differences among them exist in relation to data assimilation, initialization, and subgrid-scale parameterizations.

2. Model and observational data

The AIRS on EOS *Aqua* has observed up to 324 000 vertical profiles of T and q on a daily basis since September 2002 (Aumann et al. 2003). The retrieval approach is based on the cloud-clearing methodology (Susskind et al. 2003) and yields a nominal spatial resolution of about 45 km at nadir. The sampling, precision, and quality control of T and q are discussed in KT09, Maddy and Barnet (2008), and elsewhere. The scaling exponents (0.33, 0.5, and 1.0 in variance scaling space $\cong -5/3$, -2, and -3, respectively, in power spectral density space) are obtained by fitting power laws to observed variance spectra of T and q within $12° \times 12°$ and smaller grid boxes and on tropospheric standard pressure levels following the approach in KT09. This grid size choice resolves the mesoscale range (1.5°, 2.0°, 3.0°, 4.0°, 6.0°, and 12.0° scales) that contains the canonical -3 and $-5/3$ mesoscale break (Nastrom and Gage 1985) but also resolves regional, latitudinal, and land/ocean variations. Separate exponents are obtained for the 1.5°–4.0° (small) and 6.0°–12.0° (large) scales. The large-scale exponent is fit to fewer points than in KT09, but comparisons between this approach and KT09 exhibit virtually no difference in the derived exponent's magnitude and saves greatly on computational expense. Results herein are restricted to relatively clear skies by retaining profiles only when the AIRS total effective cloud fraction (ECF) less than 0.1 (KT09). Important AIRS sampling effects occur for larger values of ECF (Fetzer et al. 2006), in particular the lack of sampling of temperature as well as high values of water vapor within thick clouds, which may affect the interpretation of cloudy spectra. Therefore, the emphasis of this work is on atmospheric conditions best sampled by AIRS observations.

As the resolution of the AIRS operational retrieval precludes the robust calculation of variance less than 150 km in scale, we also calculate T and q spectra observed at 1-s time sampling during the VOCALS-REx campaign (Wood et al. 2011) obtained from meteorological instrumentation on the C-130 aircraft. To eliminate the confusion between horizontal geophysical variability with altitude $z_{\text{C-130}}$ ascents and descents through strong vertical gradients, spectra of T and q are restricted to

TABLE 1. Summary of weather and climate models: spatial resolution/grid configuration, data assimilation constraints, and the simulation period.

Model	Horizontal resolution	Output fields	Data assimilation?	Simulation period
GFDL C180HIRAM2.1	0.5° × 0.625°	Same	No	1 Sep–30 Nov 1995
NCAR CAM5	0.31° × 0.23°	Same	No	1 Jun–31 Aug 2005
ECMWF (CY35R2)	0.25° × 0.25°	0.5° × 0.5°	Yes	1 Jun–31 Aug 2009
MERRA	0.5° × 0.625°	1.25° × 1.25°	Yes	1 Jun–31 Aug 2009
SP-CAM	2.5° × 2.0° Embedded 2D CRM with 64 columns of 4-km resolution	Same	No	1 Sep–30 Nov in 1998–2001

horizontally level flight segments. Raw meteorological data from the C-130 were manually inspected for spurious data and inversion base crossings and these were eliminated from further consideration. Composite spectra are formed from calculating variance on flight segments of 4, 8, 16, 32, 64, 128, 256, 512, 1024, 2048, 4096, and 8192 s in time. The Lyman-α hygrometer and the Rosemount temperature probe both respond at approximately 50 Hz, which yields sufficient temporal (and thus spatial) sampling for the scales considered in this study. With a nominal flight speed of 100 m s^{-1}, this translates to distances of 0.4, 0.8, 1.6, 3.2, 6.4, 12.8, 25.6, 51.2, 102.4, 204.8, 409.6, and 819.2 km, respectively. The level flight tracks were composited into five height categories of the $z_{C\text{-}130}$ to reduce noise and geophysical variability: <0.3, 0.3–0.7, 0.7–1.5, 1.5–3.0, and >3.0 km. We obtain spectral exponents from composite spectra that are calculated from averaging flight segments with length scales of 102.4–204.8, 204.8–409.6, and 409.6–819.2 km that have at least five occurrences during VOCALS-REx. There are very few flights with longer or shorter segments and, because of a small sample size, these are less representative of the true geophysical variability of the atmosphere and thus are not included. To illustrate the tendency for a change in the scaling characteristics around the scales of the cloud features in the VOCALS-REx region (e.g., Wood and Hartmann 2006; Wood and Field 2011), two spectral exponents were separately obtained for scales less than and greater than 10 km.

Two free-running models are investigated. First, a modified version of the Geophysical Fluid Dynamics Laboratory (GFDL) Atmospheric Model version 2.1 (AM2.1) with high spatial resolution is used following Zhao et al. (2009) (see Table 1 for model details). The model is referred to as C180HIRAM2.1 and has a cubed sphere dynamical core, with 180 × 180 grid points on each face of the cube, resulting in grid sizes ranging from 43.5 to 61.6 km. In addition to changes in the dynamical core and spatial resolution, the model also differs from GFDL's AM2 model (Anderson et al. 2004) in its convection and cloud scheme (Zhao et al. 2009). Second, a modified version of the National Center for Atmospheric Research (NCAR) Community Atmosphere Model, version 5 (CAM5) with high-resolution gridding (~0.31° × 0.23°) is used (Gettelman et al. 2010). The newest version of the CAM5 includes a two-moment microphysics scheme, an updated rapid radiative transfer package, and improvements to the mixed and ice phases of clouds are obtained by including ice supersaturation and ice cloud–aerosol interactions at the point of ice nucleation. The scaling exponent calculations of T and q are described in KT09, except the boxes are 12° × 15° in the case of C180HIRAM2.1. A value of total CF < 0.5 at the top of the atmosphere (TOA) is used to screen for ''clearish'' skies, and little sensitivity of this value is reflected in the scaling exponents. The ECF from AIRS and CF from the model output are not equivalent since ECF is a convolution of cloud emissivity and coverage, whereas CF > 0 simply indicates the presence of cloud. The relative frequency of occurrences of ECF < 0.1 and CF < 0.5 are similar in magnitude and sample relatively similar spatial regimes. Results from a free-running C180HIRAM2.1 simulation during 1 September 1995–30 November 1995 for 0000 UTC snapshots, and a free-running CAM5 simulation from 1 June 2005 to 31 August 2005 for 0000 UTC snapshots, are presented in section 3.

Scaling exponents from two model analyses are also investigated. The first is the European Center for Medium-Range Weather Forecasts (ECMWF) (Jung et al. 2010) 0000 UTC analysis fields provided on a 0.5° × 0.5° grid as a part of the Year of Tropical Convection project. The model cycle is CY35R2 with a resolution of T799 (25 km) over 91 vertical levels. Several sources of data relevant to T and q are assimilated, which include Global Positioning System (GPS) occultations, radiosonde profiles, and AIRS and Infrared Atmospheric Sounding Interferometer (IASI) radiances, as well as AMSU A/B and Special Sensor Microwave Imager (SSM/I) microwave radiances. The second model analysis is the Modern Era Retrospective Analysis for Research and Applications (MERRA; http://gmao.gsfc.nasa.gov/merra/) fields at 1.25° × 1.25° resolution. Note that the native resolution of MERRA [version 5.2.0 of Goddard Earth Observing

System (GEOS-5) Data Assimilation System (DAS)] is $0.5° \times 0.625°$, similar to C180HIRAM2.1. GEOS-5 also assimilates many of the same data as ECMWF including radiosondes, AIRS, AMSU A/B, and SSM/I (Rienecker et al. 2008). As with the C180HIRAM2.1 and CAM5 models, the T and q fields are restricted to CF < 0.5. Grid box sizes of $12° \times 12°$ ($15° \times 15°$) were used for ECMWF (MERRA) and results are presented below for 1 June 2009–31 August 2009 for both models.

Lastly, variance spectra of total column water vapor (CWV) and height-resolved q from the superparameterized CAM (SP-CAM) (Marchand et al. 2009) are compared to CWV and q spectra obtained from AIRS and VOCALS-REx. Each GCM grid column of the SP-CAM is 2.5° in longitude by 2.0° in latitude and contains an embedded 2D cloud-resolving model (CRM) oriented in a west–east direction, with cyclic lateral boundary conditions within each GCM grid box. Each CRM contains 64 columns of 4-km horizontal grid size, and the variance is calculated at 8, 16, 32, 64, 128, 243, 487, 731, 975, and 1218 km once per day at 1200 UTC. The variance at scales less than 256 km is calculated from the 2D CRM fields only. Results are presented for three specific regions during 1 September–30 November 1998, 1999, 2000, and 2001.

3. Results

a. Regional vertical profiles

Figure 1 illustrates model and AIRS variance spectra for T in three different cloud regimes: stratocumulus in the southeastern Pacific (SC), trade cumulus near Hawaii (TC), and a convectively active region in the tropical western Pacific (DC). The magnitude of the AIRS T variance depends on altitude, length scale, and region (KT09). The change in the slope of the variance (i.e., ''scale break'') at 500 hPa in SC is discernible around 400–600 km but is significantly weaker in TC and essentially nonexistent in DC. A much weaker scale break is observed in the boundary layer and near the tropopause (KT09). Since the slope in the T variance is weaker at 925 hPa in SC, the relative magnitude compared to other pressure levels is significantly larger in DC, showing large low-level T variability. There is a general tendency for the model spectral slopes to be uniformly steep relative to AIRS. This translates to T variance that is similar to AIRS in the 600–1300-km length scales, and several factors less than AIRS within the 150–400-km scales, depending on the region, level, and model. This is consistent with limitations of coarsely gridded global models to generate small-scale variability in the tropics (e.g., Willett et al. 2008). The models tend to have the highest variance in the lowest levels (e.g., 925 and 850 hPa), but this behavior holds for AIRS only within DC and at the smallest length scales in other regimes. For SC, the CAM5, C180HIRAM2.1, and MERRA fields show the highest variance at 500 hPa, while ECMWF shows much greater variance at 850 and 925 hPa. ECMWF more clearly shows (as compared to other models) what would be expected, to first order, with values of variance that decrease from the boundary layer to the top of the atmosphere. However, in most instances, the relative ''ordering'' of variance by pressure level is consistent between AIRS and the various models.

In the case of q (Fig. 2), there is a notable absence of a significant scale break in the three regions in the AIRS data (e.g., KT09). The variance is clearly higher for 925 and 850 hPa in SC and TC, but not in DC. In fact, the spectral slope of q at 925 hPa in DC is much less than that at 850 and 500 hPa. Figure 2 shows an absence of a significant scale break in all models, while the model exponents are uniformly steeper than AIRS. The variance magnitudes are more similar between the models and AIRS in the case of q than T, although this is less pronounced in the DC region, especially for the free-running models that have much too little variance at small scales. The intermodel spread of the variance in the free troposphere (e.g., 500 hPa) is much higher than at 850 and 925 hPa, suggesting bigger discrepancies in the variability of water vapor in the middle troposphere between the models and AIRS observations (cf. Pierce et al. 2006), which could be associated with systematic differences in terms of deep convection representation. In all three regions, the models have a slightly higher magnitude of q variance at 850 hPa compared to 925 hPa, presumably from variations in the PBL height that lead to more variations in dry and moist occurrences at a given pressure level. However, this behavior is only observed in DC with AIRS.

The 1-σ daily variability of selected AIRS variance spectra shown in Figs. 1 and 2 is quantified in Fig. 3. All four models at various times either agree or disagree with AIRS, depending on the region of study (SC, TC, and DC), horizontal scale, and pressure level (only 500 and 850 hPa are shown for sake of clarity). Even if the power-law exponent for a particular model variance spectrum is very similar to AIRS, the magnitude of the variance may be several factors higher or lower (e.g., CAM5 q at 500 hPa in TC). The 1-σ variability is not an estimate of a systematic bias like those that result from partial AIRS sampling in cloudy scenes; this type is minimized by filtering ''cloudy'' regions in AIRS observations and model simulations. Furthermore, a CF dependence in the root-mean-square error (RMSE) of

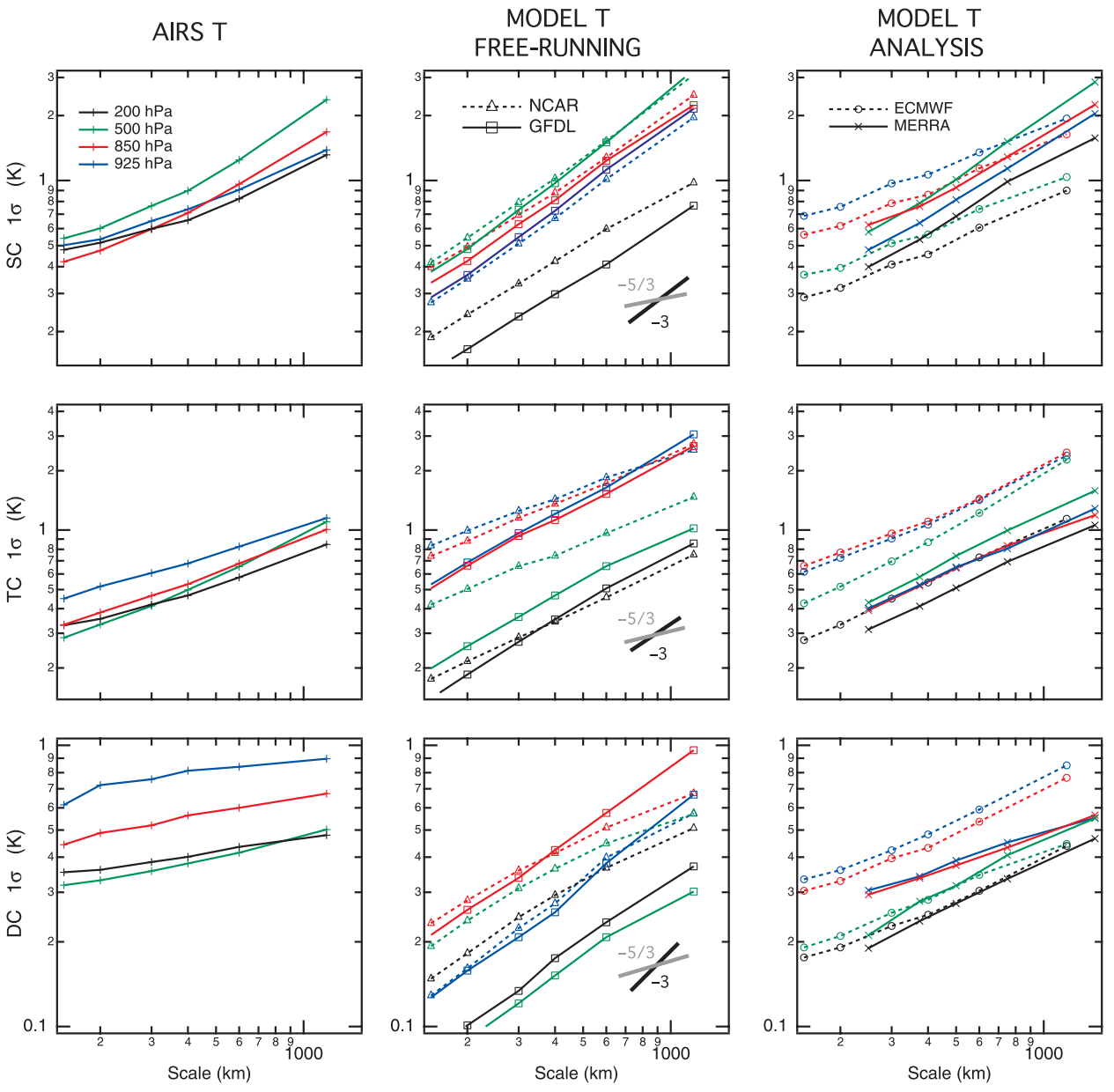

FIG. 1. Variance spectra of T for three spatial regions: southeastern Pacific stratocumulus region [24°S, 90°W (97.5°W)], trade cumulus near Hawaii [24°N, 150°W (157.5°W)], and a convective region in the tropical western Pacific [0°, 150°E (157.5°E)]. AIRS, ECMWF, and CAM5 (C180HIRAM2.1) model results contained within a 12° × 12° (12° × 15°) box centered at first (second) longitudinal value. The CAM pressure levels are located at 197.9, 524.7, 859.5, and 936.2 hPa; all other model levels are as shown in the figure legend.

AIRS T and q is significantly less than 0.1 K and less than 1%–2% of the magnitude of the mixing ratio, respectively, for values of ECF < 0.1 (Susskind et al. 2006). Therefore, no regime (or CF) dependence on the slope of the spectral variance explains the character of the spectral break observed in AIRS T. In short, comparisons of variance scaling exponents should be used in synergy with the variance magnitudes themselves and their temporal variation.

b. *Zonal averages*

Figure 4 shows the zonal averaged T and q exponents for both the large (600–1200 km) and small (150–400 km) scales. All of the models capture some aspects of the zonal structure in T observed by AIRS at the large scales including the decrease in the deep tropics for T (Nastrom and Gage 1985; Frehlich and Sharman 2010). However, the model scaling in the tropics is uniformly too large,

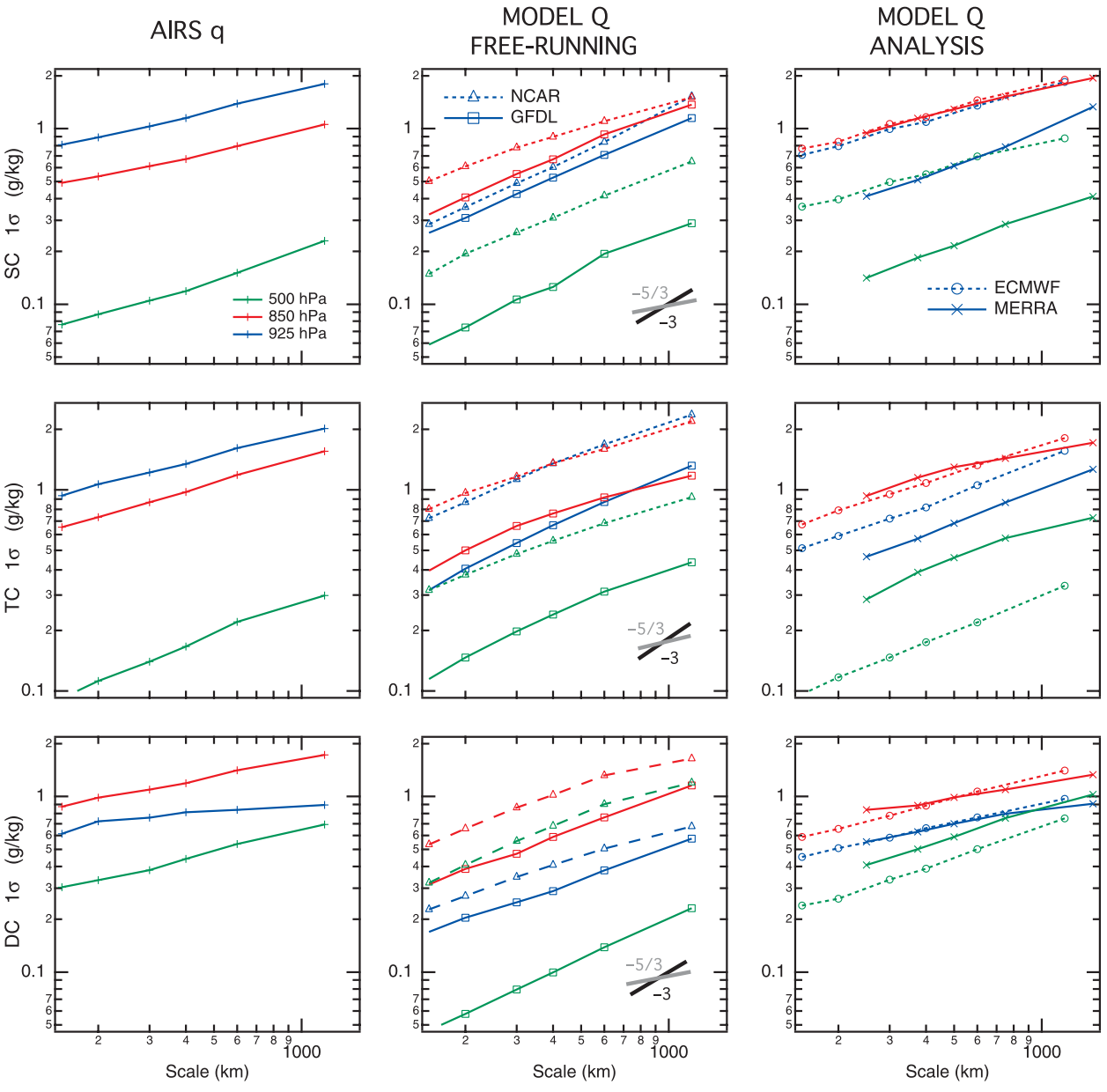

FIG. 2. As in Fig. 1, but for the quantity q (g kg^{-1}).

although ECMWF and MERRA have sharper horizontal gradients than CAM5 and C180HIRAM2.1. This is consistent with the inability of convective parameterizations in global models to generate enough small-scale variance from 100 to 500 km (Willett et al. 2008). A scale break in T is observed between the large and small scales, but the small-scale exponents are 0.1–0.3 larger than AIRS. Both ECMWF and MERRA are closer in magnitude to AIRS than CAM5 and C180HIRAM2.1 for large-scale T, but still somewhat higher than AIRS. There is a hint of a decrease in the scaling near the tropopause (Dotzek and Gierens 2008) in the large T exponents in C180HIRAM2.1, ECMWF, and MERRA. However, the CAM5 model has a rather constant increase in the scaling with distance from the equator and with altitude in large T, while C180HIRAM2.1 has a small peak near 30°N and 30°S, which is even more prominent in ECMWF and MERRA fields. For q scaling, all models show a weak to nonexistent scale break that is consistent with AIRS (KT09) and other limited aircraft observations (Nastrom et al. 1986; Cho et al. 2000). However, the model scaling is still

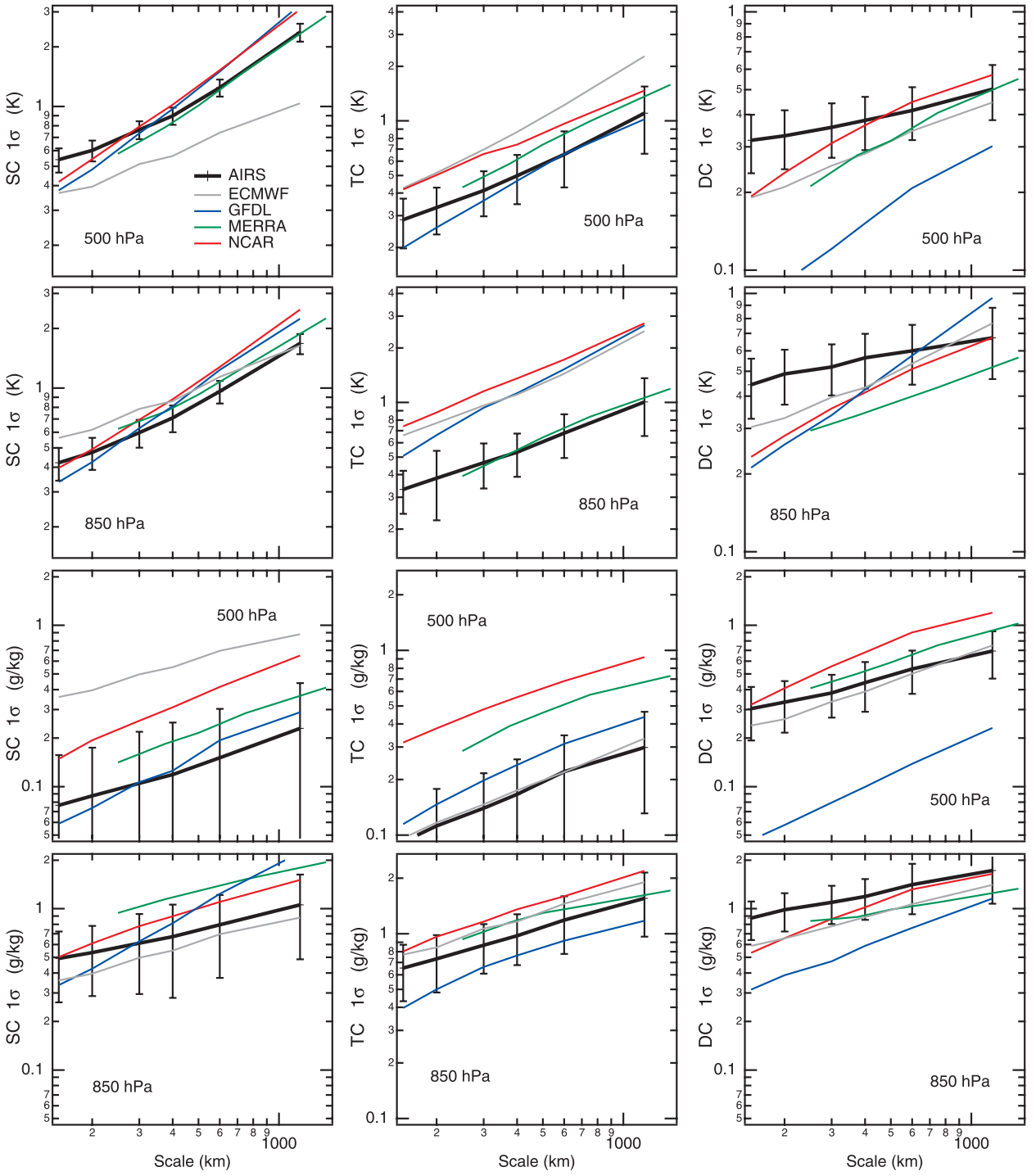

FIG. 3. Selected AIRS and climate model spectra taken from Figs. 1 and 2 for 850 and 500 hPa only. The vertical bars represent 1-σ variability taken from daily snapshots. Similar vertical bars were obtained for model spectra and are within a few factors smaller or larger in magnitude (not shown for sake of clarity).

too steep relative to AIRS outside of the tropical free troposphere. Furthermore, steeper model exponents are seen near the tropopause and near-surface layers in comparison to AIRS.

c. *SP-CAM and AIRS*

In Fig. 5, comparisons between SP-CAM and AIRS CWV are shown for three similar regions discussed in

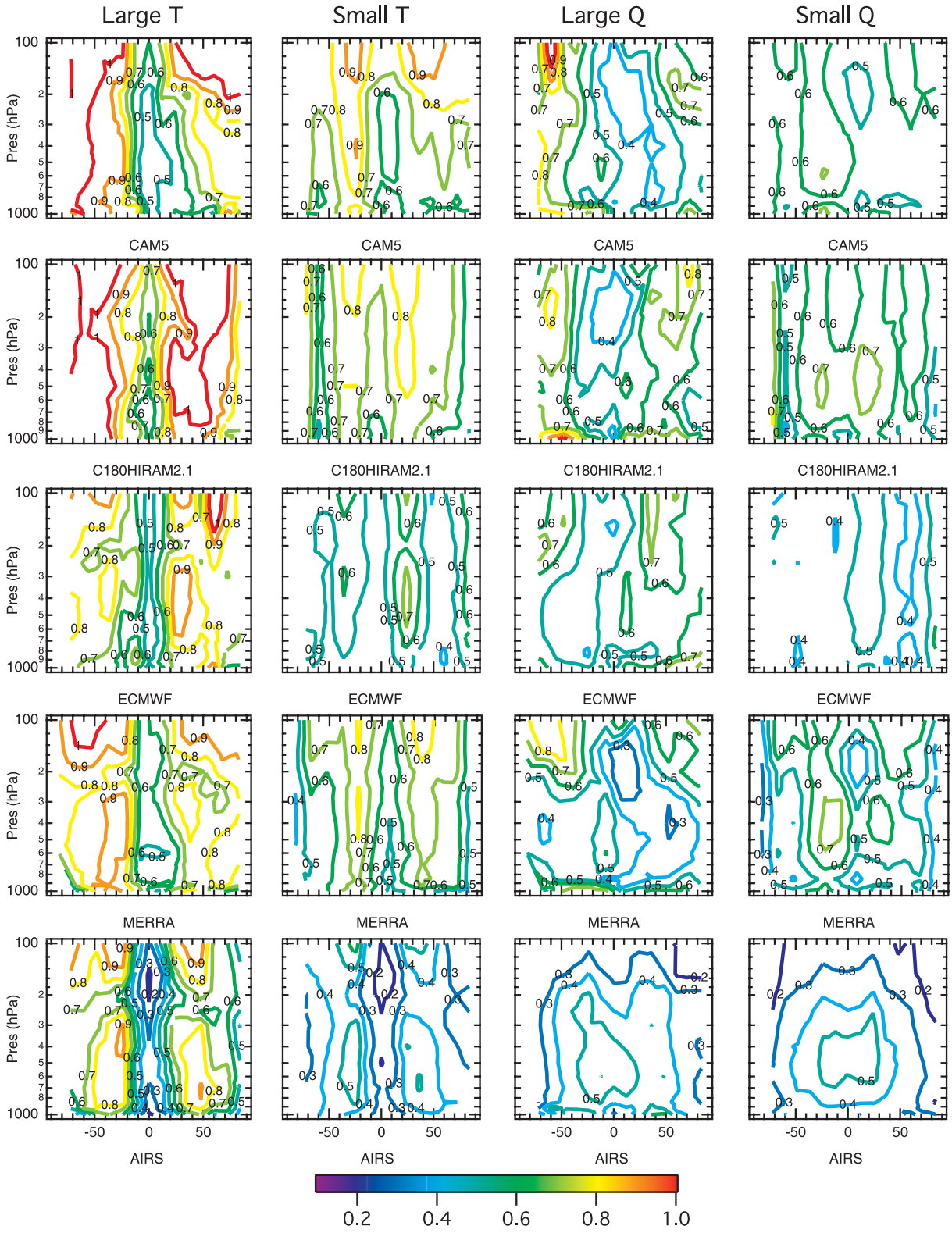

FIG. 4. Zonal averaged scaling exponents for AIRS, MERRA, ECMWF, C180HIRAM2.1, and CAM5 (left) T and (right) q for "clear sky" (see text for a description). The large (small) exponents are obtained from fitting power-law exponents restricted to 600–1200 km (150–400 km) following the methodology of KT09, except for MERRA, which are obtained from 250–500 km (750–1500 km).

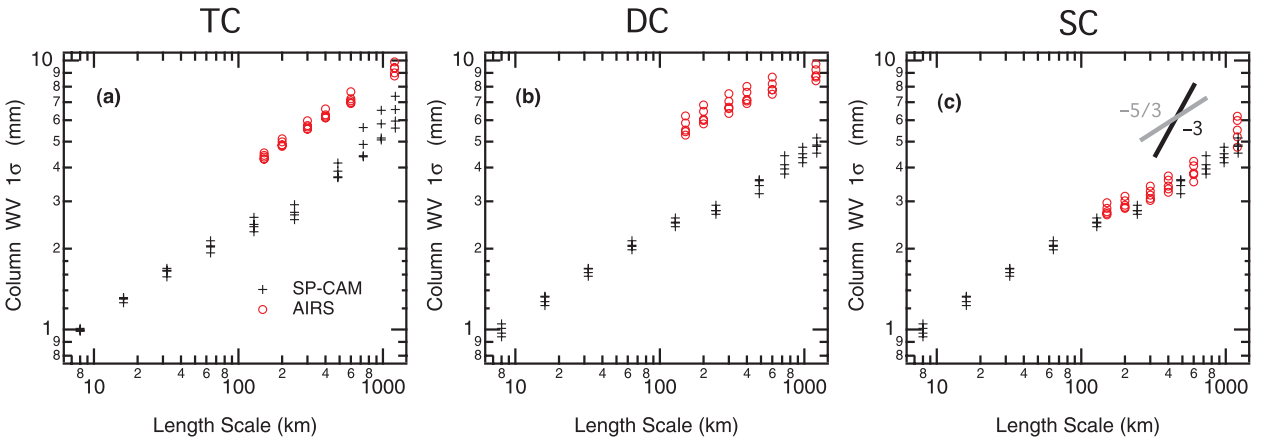

FIG. 5. Shown are CWV spectra of SP-CAM (AIRS) for three regions: (a) 10°–20°N, 157.5°–170°W (6°–18°N, 156°–168°W), (b) 4°S–6°N, 157.5°–170°E (6°S–6°N, 150°–162.5°E), and (c) 10°–20°S, 77.5°–90°W (6°–18°S, 84°–96°W). All spectra are from September–November (SON) at 1200 UTC during 1998–2001 (SP-CAM) and 0000 UTC during 2004–08 (AIRS). The scaling exponents for −5/3 (0.33) and −3 (1.0) are shown in gray (black).

Figs. 1–3. It is abundantly clear that the scaling in AIRS CWV does not behave like the height-resolved q shown in Figs. 1–4. In fact, CWV has a steeper slope at scales greater than 250 km in TC and SC compared to DC, much like the scaling of T. Thus, CWV is not an appropriate analog for layer-resolved scaling exponents of q. This emphasizes the importance of making vertically resolved q observations, and sharp differences in boundary layer (0.3) and free troposphere (0.5) exponents obtained from meteorological tower observations support this view (Pressel et al. 2010). The SP-CAM and AIRS have significant differences in both the magnitude of the variances and spectral slopes at scales greater than 100 km, with variations depending on the region, while the SP-CAM is consistently close to 0.3 at smaller scales in all three regions. It is intriguing that AIRS and SP-CAM have similar values in stratocumulus (SC) and AIRS is clearly larger in deep convective (DC) regimes. In SC, most of the water vapor is in the cloudy PBL, where both AIRS and SP-CAM are supposed to have some difficulties in representing reality. On one hand, the simulations are for scales greater than 100 km, which may suggest that both AIRS and SP-CAM realistically simulate some mesoscale characteristics. On the other hand, SP-CAM is supposed to be particularly well suited for DC regions, where its low bias of CWV variance compared to AIRS is indeed puzzling. There is a scale break ~100 km simulated in SP-CAM that is not testable with the current operational AIRS retrieval because of resolution limitations (although future advancements in single AIRS field-of-view retrievals will improve this by a factor of 3). Furthermore, the scaling exponents are more variable between the different years at the larger scales in SP-CAM compared to the smaller scales, highlighting the importance of monitoring these variations with continuous, multiyear observations of interannual variability now available from AIRS.

Height-resolved q spectra from SP-CAM for the 929-, 867-, and 600-hPa levels are shown in Fig. 6. The AIRS q spectra for 925, 850, and 500 hPa from Fig. 2 are also shown in Fig. 6 for comparison. The slope of the SP-CAM is much too shallow at all scales, as the slope is essentially flat for all three regions and pressure levels at scales less than 250 km, implying pseudoscale invariance of q variability. Previous work suggests that the large discrepancy in q variance at small scales may be related to geometrical effects (2D versus 3D modeling). However, Moeng et al. (2004) found that 2D simulations of vertical moisture fluxes $\langle w'q' \rangle$ are represented fairly well in comparison to 3D models. Assuming this is also true in the SP-CAM (recall that SP-CAM is a 3D global model with an embedded 2D CRM), vertical moisture fluxes are proportional to correlations between vertical velocity $\langle w'w' \rangle$ and moisture $\langle q'q' \rangle$ variances, thus excessive $\langle q'q' \rangle$ can be compensated by either weaker $\langle w'w' \rangle$ or weaker correlations between $\langle w'w' \rangle$ and $\langle q'q' \rangle$. Some evidence for contributions from reduced $\langle w'w' \rangle$ is supported by steeper power spectra of vertical velocity in 2D compared to 3D CRMs (Moeng et al. 2004; cf. their Fig. 11). Furthermore, Bogenschutz (2011) shows that the SP-CAM has essentially no subgrid-scale turbulent fluxes, which are entirely manifested by the resolved scales. When the horizontal grid size is 4 km, the smallest scales that are effectively resolved are ~15 km. Vertical velocities at these scales are much smaller than those at subgrid scales that actually carry out these fluxes, so the resolved variances should be much larger. Modeling comparisons between 2D and

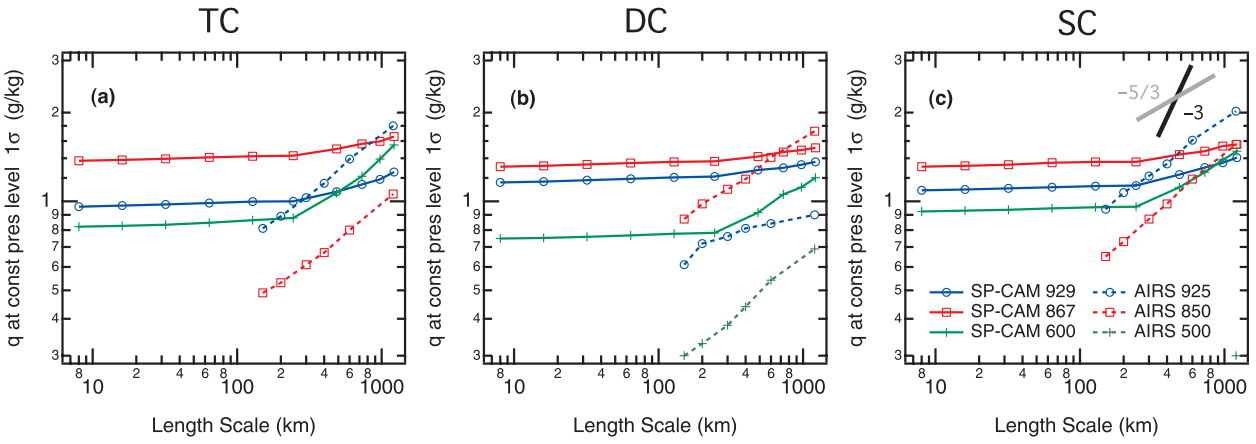

FIG. 6. As in Fig. 5, but 1-σ values of q shown at constant pressure levels in SP-CAM and AIRS.

3D CRMs, and a rigorous evaluation of the model variances and fluxes, warrants further investigation.

d. VOCALS-REx

In Fig. 7, height-resolved composite spectra of T and q obtained from VOCALS-REx from 30 to 200 km have spectral slopes similar to AIRS (Fig. 2); however, the slopes are significantly steeper at scales less than 10–20 km. The steepening at small scales is reminiscent to slopes steeper than $-5/3$ observed in boundary layer observations of q reported by Schmitt et al. (1979) and Zhang (2010) and liquid water content (Davis et al. 1996). Furthermore, spectra of T and q obtained from surface buoy data during the East Pacific Investigation of Climate (EPIC) experiment show mesoscale breaks around 20–30 km, although the spectral slopes are less steep than shown in Fig. 7 and are around 0.3–0.5 (Comstock et al. 2005). This is not unexpected as these observations are obtained from a buoy near the surface of the ocean where the scaling is expected to be weaker. All spectra at scales less than 10–20 km have increased spectral slopes and are at a minimum for $z < 300$ m ($\sim$0.4) and a maximum for $z > 1000$ m. The exponents for q are steeper than T in the free troposphere. The T spectra have a scale break $\sim$20 km as with q but it is more or less pronounced depending on the altitude. Since there are a limited number of flight segments at a constant altitude, these composite spectra may not represent the full geophysical variability in this region. However, the distinct change in spectral slopes above and below the inversion base is consistent with AIRS (KT09) and observed vertical structure in surface-based tower (Pressel et al. 2010) observations. This points to a need for more aircraft observations of thermodynamic variability in the cloudy boundary layer, and data obtained from past aircraft campaigns should be revisited to examine scale-dependent features in T and q.

4. Discussion and conclusions

Excessively large finescale variability simulated in SP-CAM and observed scale breaks in aircraft data (VOCALS-REx) are located at spatial scales unresolved by current sounders such as AIRS and the Infrared Atmospheric Sounding Interferometer (IASI), or future sounders such as the Cross-Track Infrared Microwave Sounder Suite (CrIMSS), with nominal horizontal resolutions on the order of 50 km. These scale breaks imply that extending variance to smaller scales using exponents obtained from scales resolved by these coarser-resolution sounders is not necessarily appropriate as suggested by KT09. Observing systems with sufficient spatial resolution (roughly 1–10 km horizontally) that are able to resolve dominant scales of cloud structures (Wood and Field 2011) are needed to quantify the character of the variability in different cloud regimes for all relevant geophysical variables (Stevens and Feingold 2009), not only T and q. The problem of extending variance to small scales is highly relevant to promising subgrid-scale cloud parameterization approaches that have not been fully exploited to date (e.g., Cusack et al. 1999; Tompkins 2002; Kuwano-Yoshida et al. 2010). Small-scale observations are also important for evaluating the new generation of multiscale modeling framework models (e.g., SP-CAM), global CRMs (e.g., Hamilton et al. 2008), and large-eddy simulation (LES) models (e.g., Siebesma et al. 2003).

The scaling exponents are found to be steeper in both the free-running models (CAM5 and C180HIRAM2.1) and analyses (ECMWF and MERRA) in comparison to AIRS, suggesting that the small-scale variance in these models is too small. It is not known whether this behavior is driven (in part, or in whole) by differences in subgrid-scale parameterizations (e.g., Hamilton et al. 2008), resolution (Boville 1991), differences in the

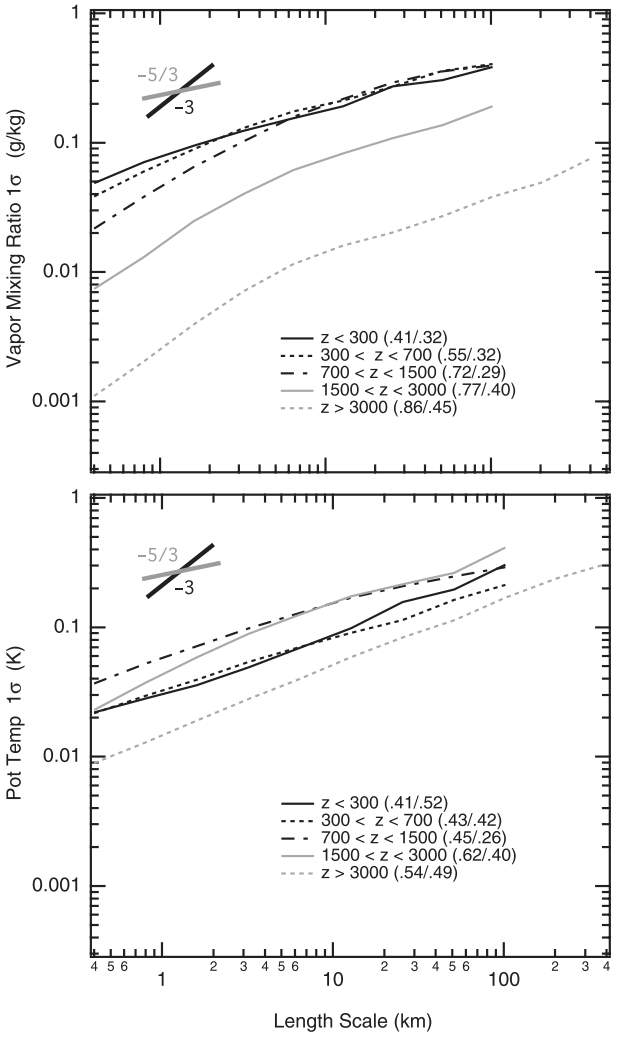

FIG. 7. Shown are composite variance spectra for (top) q and (bottom) θ in five altitude bins during VOCALS-REx for flight segments with at least five segments averaged (see text). The numbers in the parentheses are scaling exponents for spectra < 10 km on the left (> 10 km on the right).

numerical representation of the dynamical core (e.g., Rood 1987; Rasch et al. 2006; Williamson 2007), data assimilation (satellite, radiosonde, and surface observations), or other reasons, which warrants further investigation. However, it appears that the free-running models used in climate assessments have a poorer representation of the scale dependence of T and q variance than models with data assimilation systems (e.g., ECMWF and MERRA). This is qualitatively consistent with slightly poorer performance of climate models that are executed in ''weather forecast mode'' when compared to NWP models (Phillips et al. 2004); however, it is yet to be determined if small-scale variability is a primary factor in these differences of forecast skill. More research is necessary to determine the potential implications for climate sensitivity (e.g., Seiffert and von Storch 2008) and cloud feedback sign and magnitude, which include tests of ECMWF and MERRA without realistic initialization. Additional studies such as Cusack et al. (1999) that use constraints on subgrid-scale variability obtained from observations should be undertaken. As the SP-CAM results indicate, having embedded CRMs that serve as subgrid-scale parameterizations does not necessarily ensure realistic q spectra. Observational constraints from satellite and aircraft observations will continue to play an indispensable role in parameterization development and improvement efforts.

This work shows that higher horizontal spatial resolution observations of T and q over the entire globe are necessary to observe the global characteristics of small-scale ''turbulence'' in thermodynamic profiles. At the same time, current and future operational and research atmospheric sounders will continue to play a role in assessing climate processes, establishing quantitative benchmarks for model comparisons; facilitate the development of more rigorous observationally based subgrid-scale parameterizations; and possibly offer a long-term strategy to monitor regional variations in the mesoscale spectrum of T and q over the entire globe. The mesoscale spectrum observed by AIRS is broadly consistent with previous observational, theoretical, and modeling studies that demonstrate a scaling ''break'' from -3 to $-5/3$ in the neighborhood of 400–800 km in horizontal scale. However, the scale break is only observed in temperature (not height-resolved water vapor), and is most pronounced in the extratropics between the surface boundary layer and a few kilometers below the tropopause. Temperature and water vapor profiles are ''retrieved'' from observed radiances emitted from three-dimensional volumes of atmosphere (40 km or larger horizontally, 2–3 km vertically). Although this observational approach is fundamentally different than the in situ sampling and observational strategy of aircraft investigations, it offers an independent set of observations that verify the existence and quantify the magnitude of the mesoscale break in atmospheric temperature (Lovejoy et al. 2009; Lindborg et al. 2010).

As shown by Hamilton et al. (2008), the observed KE spectrum serves as a useful diagnostic for climate model assessments. We suggest that height- and regime-resolved spectra of T and q should also serve as model diagnostics as they can be highly variable in space and time. Additional A-Train datasets should serve as benchmarks for other model-relevant variables such as cloud water content and precipitation. Furthermore, their simultaneous observation with T and q can be combined into multisensor

observational estimates of moist conserved thermodynamic variables that will be directly comparable to fundamental model parameters.

Acknowledgments. Support from the JPL Internal Research and Technology Development Program, NASA's Making Earth Science Data Records for Use in Research Environments (MEaSUREs) program, and the AIRS Project at JPL is acknowledged. JT acknowledges the support provided by the Office of Naval Research, Marine Meteorology Program under award N0001408IP20064, the NASA MAP Program, and the NOAA MAPP/CPO Program. The work of X. L. Huang is partly supported by NSF Grant ATM0755310. RW acknowledges the support of VOCALS NSF Award ATM-0745702. AIRS data were obtained through the Goddard Earth Sciences Data and Information Services Center (http://daac.gsfc.nasa.gov/). ECMWF data are provided in coordination with the Year of Coordinated Observing Modeling and Forecasting Tropical Convection project (http://data-portal.ecmwf.int/data/d/yotc_od/). MERRA data are provided by the Global Modeling and Assimilation Office (http://gmao.gsfc.nasa.gov/). This material is partly based on work supported by the National Science Foundation Science and Technology Center for Multi-Scale Modeling of Atmospheric Processes, managed by Colorado State University under cooperative agreement ATM-0425247. Roger Marchand provided the SP-CAM output. The MMF model runs were performed at the Department of Energy Pacific Northwest National Laboratory (PNNL) and the San Diego Supercomputing Center (SDSC). The authors thank Stephen Eckermann, Jon Petch, Kyle Pressel, Richard Rood, Allen Schanot, Ka-Kit Tung, and the anonymous reviewers for insightful discussions and suggestions. This research was carried out at the Jet Propulsion Laboratory, California Institute of Technology, under a contract with NASA.

REFERENCES

Anderson, J. L., and Coauthors, 2004: The New GFDL global atmosphere and land model AM2–LM2: Evaluation with prescribed SST simulations. *J. Climate,* **17,** 4641–4673.

Aumann, H. H., and Coauthors, 2003: AIRS/AMSU/HSB on the Aqua mission: Design, science objectives, data products, and processing systems. *IEEE Trans. Geosci. Remote Sens.,* **41,** 253–264.

Bogenschutz, P. A., 2011: Improving the representation of turbulence and clouds in cloud resolving models and general circulation models. Ph.D. dissertation, University of Utah, 320 pp.

Bony, S., and J. L. Dufresne, 2005: Marine boundary layer clouds at the heart of tropical cloud feedback uncertainties in climate models. *Geophys. Res. Lett.,* **32,** L20806, doi:10.1029/2005GL023851.

Boville, B. A., 1991: Sensitivity of simulated climate to model resolution. *J. Climate,* **4,** 469–485.

Cahalan, R. F., W. Ridgway, W. J. Wiscombe, T. L. Bell, and J. B. Snider, 1994: The albedo of fractal stratocumulus clouds. *J. Atmos. Sci.,* **51,** 2434–2455.

Cho, J. Y. N., R. E. Newell, and G. W. Sachse, 2000: Anomalous scaling of mesoscale tropospheric humidity fluctuations. *Geophys. Res. Lett.,* **27,** 377–380.

Comstock, K. K., C. S. Bretherton, and S. E. Yuter, 2005: Mesoscale variability and drizzle in southeast Pacific stratocumulus. *J. Atmos. Sci.,* **62,** 3792–3807.

Cusack, S., J. M. Edwards, and R. Kershaw, 1999: Estimating the subgrid variance of saturation, and its parametrization for use in a GCM cloud scheme. *Quart. J. Roy. Meteor. Soc.,* **125,** 3057–3076.

Davis, A. B., A. Marshak, W. Wiscombe, and R. Cahalan, 1996: Scale invariance of liquid water distributions in marine stratocumulus. Part I: Spectral properties and stationarity issues. *J. Atmos. Sci.,* **53,** 1538–1558.

Dotzek, N., and K. Gierens, 2008: Instantaneous fluctuations of temperature and moisture in the upper troposphere and tropopause region. Part 2: Structure functions and intermittency. *Meteor. Z.,* **17,** 323–337.

Fetzer, E. J., B. H. Lambrigtsen, A. Eldering, H. H. Aumann, and M. T. Chahine, 2006: Biases in total precipitable water vapor climatologies from Atmospheric Infrared Sounder and Advanced Microwave Scanning Radiometer. *J. Geophys. Res.,* **111,** D09S16, doi:10.1029/2005JD006598.

Frehlich, R., and R. Sharman, 2010: Climatology of velocity and temperature turbulence statistics determined from rawinsonde and ACARS/AMDAR data. *J. Appl. Meteor. Climatol.,* **49,** 1149–1169.

Gettelman, A., and Coauthors, 2010: Global simulations of ice nucleation and ice supersaturation with an improved cloud scheme in the Community Atmosphere Model. *J. Geophys. Res.,* **115,** D18216, doi:10.1029/2009JD013797.

Hamilton, K., Y. O. Takahashi, and W. Ohfuchi, 2008: Mesoscale spectrum of atmospheric motions investigated in a very fine resolution global general circulation model. *J. Geophys. Res.,* **113,** D18110, doi:10.1029/2008JD009785.

Jung, T., and Coauthors, 2010: The ECMWF model climate: Recent progress through improved physical parameterizations. *Quart. J. Roy. Meteor. Soc.,* **136,** 1145–1160, doi:10.1002/qj.634.

Kahn, B. H., and J. Teixeira, 2009: A global climatology of temperature and water vapor variance scaling from the Atmospheric Infrared Sounder. *J. Climate,* **22,** 5558–5576.

Kawai, H., and J. Teixeira, 2010: Probability density functions of liquid water path and cloud amount of marine boundary layer clouds: Geographical and seasonal variations and controlling meteorological factors. *J. Climate,* **23,** 2079–2092.

Koshyk, J. N., K. Hamilton, and J. D. Mahlman, 1999: Simulation of the $k^{-5/3}$ mesoscale spectral regime in the GFDL SKYHI general circulation model. *Geophys. Res. Lett.,* **26,** 843–846.

Kuwano-Yoshida, A., T. Enomoto, and W. Ohfuchi, 2010: An improved PDF cloud scheme for climate simulations. *Quart. J. Roy. Meteor. Soc.,* **136,** 1583–1597, doi:10.1002/qj.660.

Lindborg, E., 2009: Two comments on the surface quasigeostrophic model for the atmospheric energy spectrum. *J. Atmos. Sci.,* **66,** 1069–1072.

——, K. K. Tung, G. D. Nastrom, J. Y. N. Cho, and K. S. Gage, 2010: Comment on ''Reinterpreting aircraft measurement in anisotropic scaling turbulence'' by Lovejoy et al. (2009). *Atmos. Chem. Phys.,* **10,** 1401–1402.

Lovejoy, S., A. F. Tuck, D. Schertzer, and S. J. Hovde, 2009: Reinterpreting aircraft measurements in anisotropic scaling turbulence. *Atmos. Chem. Phys.,* **9,** 5007–5025.

Maddy, E. S., and C. D. Barnet, 2008: Vertical resolution estimates in version 5 of AIRS operational retrievals. *IEEE Trans. Geosci. Remote Sens.,* **46,** 2375–2384.

Marchand, R., N. Beagley, and T. P. Ackerman, 2009: Evaluation of hydrometeor occurrence profiles in the Multiscale Modeling Framework climate model using atmospheric classification. *J. Climate,* **22,** 4557–4573.

Moeng, C.-H., J. C. McWilliams, R. Rotunno, P. P. Sullivan, and J. Weil, 2004: Investigating 2D modeling of atmospheric convection in the PBL. *J. Atmos. Sci.,* **61,** 889–903.

Nastrom, G. D., and K. S. Gage, 1985: A climatology of atmospheric wavenumber spectra of wind and temperature observed by commercial aircraft. *J. Atmos. Sci.,* **42,** 950–960.

——, W. H. Jasperson, and K. S. Gage, 1986: Horizontal spectra of atmospheric tracers measured during the global atmospheric sampling program. *J. Geophys. Res.,* **91,** 13 201–13 209.

Phillips, T. J., and Coauthors, 2004: Evaluating parameterizations in general circulation models: Climate simulation meets weather prediction. *Bull. Amer. Meteor. Soc.,* **85,** 1903–1915.

Pierce, D. W., T. P. Barnett, E. J. Fetzer, and P. J. Gleckler, 2006: Three-dimensional tropospheric water vapor in coupled climate models compared with observations from the AIRS satellite system. *Geophys. Res. Lett.,* **33,** L21701, doi:10.1029/2006GL027060.

Pressel, K. G., W. D. Collins, and A. R. Desai, 2010: Variance scaling in water vapor measurements from a tall tower. *Extended Abstracts, 13th Conf. on Cloud Physics,* Portland, OR, Amer. Meteor. Soc., P1.77. [Available online at http://ams.confex.com/ams/13CldPhy13AtRad/techprogram/paper_171839.htm.]

Randall, D. A., and Coauthors, 2007: Climate models and their evaluation. *Climate Change 2007: The Physical Science Basis,* S. Solomon et al., Eds., Cambridge University Press, 589–662.

Rasch, P. J., D. B. Coleman, N. Mahowald, D. L. Williamson, S.-J. Lin, B. A. Boville, and P. Hess, 2006: Characteristics of atmospheric transport using three numerical formulations for atmospheric dynamics in a single GCM framework. *J. Climate,* **19,** 2243–2266.

Rienecker, M. M., and Coauthors, 2008: The GEOS-5 data assimilation system—Documentation of versions 5.0.1, 5.1.0, and 5.2.0. NASA Tech. Rep. TM-2008-104606, Vol. 27, 118 pp.

Rood, R. B., 1987: Numerical advection algorithms and their role in atmospheric transport and chemistry models. *Rev. Geophys.,* **25,** 71–100.

Schmitt, K. F., C. A. Friehe, and C. H. Gibson, 1979: Structure of marine surface layer turbulence. *J. Atmos. Sci.,* **36,** 602–618.

Seiffert, R., and J.-S. von Storch, 2008: Impact of atmospheric small-scale fluctuations on climate sensitivity. *Geophys. Res. Lett.,* **35,** L10704, doi:10.1029/2008GL033483.

Siebesma, A. P., and Coauthors, 2003: A large eddy simulation intercomparison study of shallow cumulus convection. *J. Atmos. Sci.,* **60,** 1201–1219.

Skamarock, W. C., 2004: Evaluating mesoscale NWP models using kinetic energy spectra. *Mon. Wea. Rev.,* **132,** 3019–3032.

Smith, K. S., and R. Tulloch, 2009: Reply. *J. Atmos. Sci.,* **66,** 1073–1076.

Stevens, B., and G. Feingold, 2009: Untangling aerosol effects on clouds and precipitation in a buffered system. *Nature,* **461,** 607–613.

Susskind, J., C. D. Barnet, and J. M. Blaisdell, 2003: Retrieval of atmospheric and surface parameters from AIRS/AMSU/HSB data in the presence of clouds. *IEEE Trans. Geosci. Remote Sens.,* **41,** 390–409.

——, ——, ——, L. Iredell, F. Keita, L. Kouvaris, G. Molnar, and M. Chahine, 2006: Accuracy of geophysical parameters derived from Atmospheric Infrared Sounder/Advanced Microwave Sounding Unit as a function of fractional cloud cover. *J. Geophys. Res.,* **111,** D09S17, doi:10.1029/2005JD006272.

Takahashi, Y. O., K. Hamilton, and W. Ohfuchi, 2006: Explicit global simulation of the mesoscale spectrum of atmospheric motions. *Geophys. Res. Lett.,* **33,** L12812, doi:10.1029/2006GL026429.

Tompkins, A. M., 2002: A prognostic parameterization for the subgrid-scale variability of water vapor and clouds in large-scale models and its use to diagnose cloud cover. *J. Atmos. Sci.,* **59,** 1917–1942.

Tuck, A. F., 2010: From molecules to meteorology via turbulent scale invariance. *Quart. J. Roy. Meteor. Soc.,* **136,** 1125–1144, doi:10.1002/qj.644.

Tulloch, R., and K. S. Smith, 2006: A theory for the atmospheric energy spectrum: Depth-limited temperature anomalies at the tropopause. *Proc. Natl. Acad. Sci. USA,* **103,** 14 690–14 694.

Tung, K. K., and W. W. Orlando, 2003: The k^{-3} and $k^{-5/3}$ energy spectrum of atmospheric turbulence: Quasigeostrophic two-level model simulation. *J. Atmos. Sci.,* **60,** 824–835.

Wang, H., G. Feingold, R. Wood, and J. Kazil, 2010: Modelling microphysical and meteorological controls on precipitation and cloud cellular structures in southeast Pacific stratocumulus. *Atmos. Chem. Phys.,* **10,** 6347–6362.

Willett, M. R., P. Bechtold, D. L. Williamson, J. C. Petch, S. F. Milton, and S. J. Woolnough, 2008: Modeling suppressed and active convection: Comparisons between three global atmospheric models. *Quart. J. Roy. Meteor. Soc.,* **134,** 1881–1896, doi:10.1002/qj.317.

Williamson, D. L., 2007: The evolution of dynamical cores for global atmospheric models. *J. Meteor. Soc. Japan,* **85B,** 241–269.

Wood, R., and D. L. Hartmann, 2006: Spatial variability of liquid water path in marine low cloud: The importance of mesoscale cellular convection. *J. Climate,* **19,** 1748–1764.

——, and P. R. Field, 2011: The distribution of cloud horizontal sizes. *J. Climate,* in press.

——, ——, and W. R. Cotton, 2002: Autoconversion rate bias in stratiform boundary layer cloud parameterizations. *Atmos. Res.,* **65,** 109–128.

——, and Coauthors, 2011: The VAMOS Ocean–Cloud–Atmosphere–Land Study Regional Experiment (VOCALS-REx): Goals, platforms, and field operations. *Atmos. Chem. Phys.,* **11,** 627–654.

Zhang, J. A., 2010: Spectral characteristics of turbulence in the hurricane boundary layer over the ocean between the outer rain bands. *Quart. J. Roy Meteor. Soc.,* **136,** 918–926, doi:10.1002/qj.610.

Zhao, M., I. M. Held, S.-J. Lin, and G. A. Vecchi, 2009: Simulations of global hurricane climatology, interannual variability, and response to global warming using a 50-km resolution GCM. *J. Climate,* **22,** 6653–6678, doi:10.1175/2009JCLI3049.1.